Mid- and Near-Infrared Spectra of Conformers of H-Pro-Trp-OH

Thomas Häber, Kai Seefeld, and Karl Kleinermanns*

Institut für Physikalische Chemie, Heinrich-Heine Universität Düsseldorf, 40225 Düsseldorf, Germany

Received: January 23, 2007; In Final Form: February 27, 2007

We present near- and mid-infrared−UV double resonance spectra of the natural dipeptide H−Pro-Trp−OH. Two conformers are present in the supersonic expansion: a stretched conformer with fully extended backbone and a folded conformer with an $OH\cdots OC_{pep}$ hydrogen bond. Both conformers are stabilized by dispersion interaction between indole ring and peptide backbone and a $NH_{pep}/N_{proline}$ contact. The vibrational and conformational assignment is supported by DFT and MP2 calculations. An adequate description of the energetic order of different conformers requires the explicit inclusion of dispersion and geometry optimization at the MP2 level. We will address the very sensitivity of the observed conformations to the structure of the end groups.

1. Introduction

The formation of secondary structures is the first step in the folding process of proteins and depends on numerous factors such as intra- and intermolecular hydrogen bonds (among residues and with the solvent), van der Waals and electrostatic interactions, as well as entropic effects.[1,2] Gas-phase studies of small biomolecules provide a unique way to investigate the intrinsic molecular properties of these *biomolecular* building blocks without the influence of solvents or under size-controlled conditions by adding a definite number of water molecules, summarized in a number of recent reviews.[3−7] Such studies provide useful information about the interactions responsible for the different kinds of structural motifs like β-sheets, α-helices and tight turns. In this field, UV/UV and IR/UV double resonance methods[5] are of special importance, because of the unprecedented mass and conformational selectivity, combined with sufficiently high spectral resolution to allow for a direct comparison with high level ab initio calculations.[8−17] After the pioneering work of Levy and co-workers on tryptophane,[18,19,20] a number of papers concerning amino acids,[21−27] natural and capped (model) di- and tripeptides,[9,10,28−37] and β-sheet models[38−43] were published.

However, when studying model peptides, one always has to consider end group effects, whether in natural or capped peptides, because end groups can impose specific local conformations in small model peptides other than that observed in a natural peptide chain, i.e., when the end groups themselves are part of the hydrogen bonds and not simple spectators. The existence of a strong sequence dependence on the local conformations of phenylalanine and tryptophane containing dipeptides demonstrate such effects nicely.[7,30−33] Therefore, it is not trivial to study the *real* intrinsic folding properties of the peptide backbone by investigating model systems. In fact we observe first the intrinsic properties of the isolated model system in the gas-phase. The sum of all studies on different types of model systems will then give us a very good picture of the involved kinds of interactions, the driving forces and provide stringent tests for theory. Only that combination might enable us to better understand the folding properties of proteins. It should be noted that the hydrogen bonded conformer is not necessarily the dominant species found in supersonic expansions, in spite of the flexibility of the carboxylic OH group in natural (uncapped) peptides and the strength of an $OH\cdots OC_{pep}$ hydrogen bond.[8,30,31]

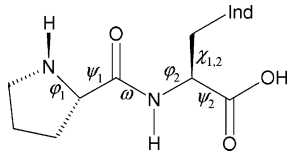

Figure 1. Structure of H−Pro-Trp−OH and angles used to describe the different conformers.

In this work we present the IR/UV spectra of the dipeptide H−Pro-Trp−OH (from now on labeled ProTrp). Proline is the only amino acid with a secondary amino group found in proteins. The relatively rigid, five-membered pyrrolidine ring puts a rigid constraint on the $N-C_\alpha$ bond rotation and restricts the value of φ in proteins to about −60 to −75°.[2,44] Since the proline residue in proteins has no amide hydrogen, it cannot act as a hydrogen bond donor, but the peptide bond preceding the proline residue can adopt the cis configuration more easily. Proline is commonly found in β turns, as the first residue of α helices and in hydroxy polyproline helices, which is the major secondary structure in collagen. ProTrp is the first of a series of natural proline containing peptides that we will study in our lab to address the specific role of proline in proteins.

Figure 1 depicts the structure of H−Pro-Trp−OH and the dihedral angles used to characterize the different conformers, ϕ, ψ, ω, and χ. The nomenclature of the dihedral angles follows the proposal of Edsall et al.[45] ϕ and ψ are measured along the peptide backbone. The fully extended backbone corresponds to $\phi = \psi = 180°$.[2] $\chi_{1,2}$ is the first dihedral angle of the indole side chain and defined as $NC_\alpha C_\beta C_\gamma$. The amino acid residues are counted starting from the nitrogen end.

The remaining paper is organized as follows: First, a brief description of the experimental setup with an emphasis on the mid-infrared laser source and on improvements of the signal-to-noise ratio in our laser desorption measurements is given. Afterward we will present the experimental results and provide a tentative assignment of the vibrational bands, based on the

* Corresponding author. E-mail: kleinermanns@uni-duesseldorf.de.

10.1021/jp070571e CCC: $37.00
Published on Web 04/04/2007

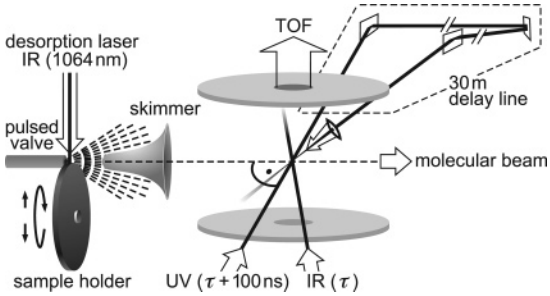

Figure 2. Experimental setup, showing the laser desorption and ionization region. The UV analysis laser travels more than 30 meters after crossing the molecular beam, then it is redirected and focused into the ionization region again to generate a reference signal of ions used to normalize the hole-burning signal.

comparison with previous studies. In the next section we will present the results of DFT calculations and ab initio calculations at the MP2 level of theory. We will mainly focus on structural principles and on how structural changes influence spectral fingerprints. Finally, we will discuss the results in the light of our previous measurements of tryptophane containing di- and tripeptides[30,32] and other proline containing model peptides.[29,32]

2. Experiment

The basic principles of our IR−UV experimental setup were described in detail elsewhere.[31,41,46,47] Here we will give a brief summary of the major components and focus on new aspects like the mid-infrared measurements and the use of a reference signal to improve the signal-to-noise ratio of our measurements.

Solid samples of ProTrp are vaporized into an argon jet by laser desorption and investigated by IR−UV hole burning spectroscopy. ProTrp (Bachem) is mixed with graphite powder (Aldrich) in a ≈1:2 ratio and applied to the edge of a 2 mm thick graphite wheel (diameter 60 mm), which is placed underneath the orifice of a 300 μm pulsed valve (General Valve). A slow rotation of the graphite wheel (1 turn per 45 min) constantly provides fresh material to be exposed to the desorption laser (Minilite, Spectra Physics, 1064 nm, ∼5 mJ/cm^2). Argon is used as carrier gas, at a stagnation pressure of 3 bar.

The skimmed molecular beam (skimmer diameter 1 mm) crosses the UV ionization laser (LAS, frequency doubled, attenuated to < 0.1 mJ/pulse) at right angle inside the ion extraction region of a linear time-of-flight (TOF) mass spectrometer in Wiley−McLaren configuration (Figure 2). A pulsed IR laser beam (burn laser) is aligned collinear to the UV beam (probe laser) and fired 100 ns before the latter. The burn laser (IR) frequency is scanned over the vibrational transitions, while the ionization laser (UV probe laser) is kept at a frequency resonant with an electronic transition of a single conformer (resonance enhanced 2-photon ionization, R2PI). Each time the burn laser excites a vibrational transition of the conformer, which is in resonance with the UV laser, the ground states get depleted, accompanied by a decrease of the corresponding mass signal, since the ionization of a vibrationally excited-state is no longer resonance enhanced at the given UV frequency. By monitoring the ion mass signal as a function of IR frequency, mass and conformer selective infrared spectra can be obtained.

IR laser light is generated by a setup originally developed by Gerhards and co-workers[47] and involves a three-stage difference frequency generation (DFG)/optical parametric amplification (OPA) setup in order to generate infrared radiation between 5 and 8 μm. Basically, a dye laser (Precision Scan, Sirah), with Styryl 8 or 9 in methanol or DMSO, is pumped by the 532 nm output of a frequency doubled Nd:YAG laser (GCR 230Pro, Spectra Physics). The dye laser output is mixed with a part of the fundamental (1064 nm) of the same Nd:YAG laser in a $LiNbO_3$ crystal for difference frequency generation, producing infrared radiation around 2.6 μm. After separating the infrared beam from the dye and Nd:YAG fundamentals by dichroic mirrors, the IR beam is mixed with the Nd:YAG fundamental in a second $LiNbO_3$ crystal, utilizing an OPA process to generate signal and idler beams at about 2.6 and 1.8 μm, respectively. Pulse energies of up to 8 mJ (idler) at a resolution of $\sim$ 0.5 cm^{-1} can be achieved with our setup. After proper rotation of the polarizations, IR radiation between 5 and 8 μm is produced in the third stage by difference frequency mixing idler and signal beams of the OPA stage in an antireflection coated $AgGaSe_2$ crystal. Energies of up to 300 μJ @ 1800 cm^{-1} can be obtained with a total incident energy of 10 mJ (signal + idler of the OPA stage) on the $AgGaSe_2$ crystal, which is sufficient for the measurement of IR/UV hole burning spectra. Because the generated mid-infrared beam is quite diverging, it has to be focused into the ion extraction region by a 60 cm focal length lens.

The ro-vibrational transitions of the water bending (1595 cm^{-1}) and stretching vibrations (3657 and 3756 cm^{-1}) were used for frequency calibration. Up to now, our IR laser system is operated unpurged, therefore absorption bands of the water stretching vibrations are visible in the mid-infrared region as well, because of atmospheric water absorptions in the first DFG and OPA stage. A disadvantage of the unpurged operation is the strong atmospheric absorption along the path length of the mid-infrared beam between laser source and apparatus (about 1.5 m), resulting in a decrease of the mid-infrared pulse energy to less than 50 μJ at certain frequencies. Nonetheless, IR spectra of laser-desorbed molecules and good signal-to-noise ratio can be obtained even with an unpurged system. The problem of atmospheric water absorptions will be discussed later and a purging system will be installed shortly. We did not normalize the infrared spectra to the IR laser energy.

A major source of noise in laser desorption experiments are shot-to-shot fluctuations of the number of desorbed molecules. These might be caused by an inhomogeneous coating of the graphite wheel, pulse-to-pulse fluctuations of the desorption laser energy, or an inhomogeneous heating of the graphite wheel and graphite/substrate mixture at different positions on the wheel. Intensity noise due to shot-to-shot fluctuations can largely be compensated by creating a reference signal: We redirect and focus the same UV laser pulse, we used to ionize the molecules into the sample region again. After passing a 30 m delay line, it causes a second ion signal to appear ∼100 ns after the first. Because the redirected beam is focused, its interaction volume with the IR beam is small and the corresponding ion signal reflects mostly nonresonant ionization; hence, it shows only a small IR dip, if at all. The reference signal is scaled then to match the baseline of the first ion signal and subtracted from the latter. Since both ion signals originate from the very same laser pulse and sample the same gas pulse, common noise due to energy and number density fluctuations are mostly eliminated in the resulting signal. An increase of the signal-to-noise ratio by a factor of $\sim$ 4 could be obtained.

3. Results

Previously, we published R2PI spectra of ProTrp in the wavenumber range between 34650 and 35100 cm^{-1}.[35] In that frequency range, UV−UV hole-burning spectra revealed the existence of two conformers, A and B. (From now on we will use capital letters A and B for the experimentally determined

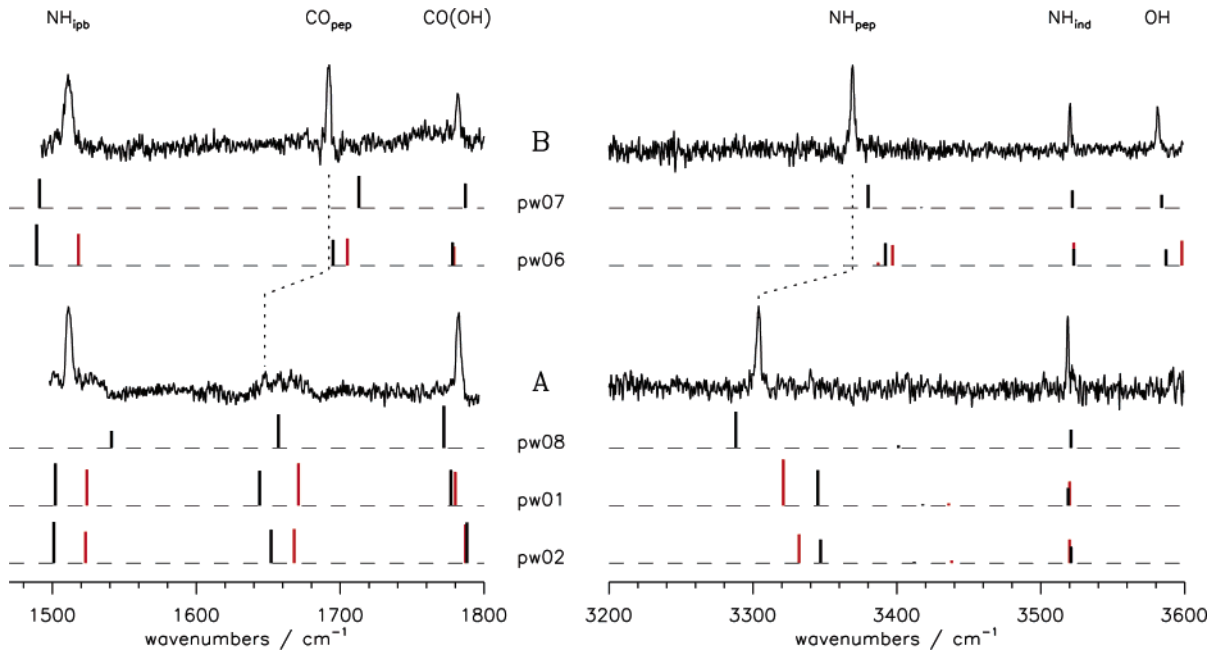

Figure 3. IR/UV double resonance spectra of both conformers of ProTrp(A and B[35]) in the mid (left) and near-infrared (right). Assignments are indicated by the labels on top and dotted lines. See text for more details. Laser pulse energies ranged between 50−300 μJ and 1−2 mJ in the mid and near-infrared, respectively, with an UV analysis laser pulse of about 10−20 μJ. Also shown are the calculated and scaled stick spectra of selected calculated conformers at the DFT (black) and MP2 (red) level of theory, ordered in groups according to an increasing MP2 energy (from bottom to top) for each experimental conformer.

TABLE 1: Experimentally Determined IR Band Maxima (in cm^{-1}) of the Two Conformers of ProTrp

vibration	conformer A	conformer B
OH		3582
NH_{ind}	3519	3520
NH_{pep}	3304	3369
CO(OH)	1782	1782
CO_{pep}	(1648)[a]	1692
NH_{ipb}	1511	1511

[a] The CO_{pep} band of conformer A was obscured by a strong water absorption, reducing the IR pulse energy at that frequency to about 50 μJ (see text for details).

conformers.) Their apparent electronic origins had a spacing of about 160 cm^{-1}. In the same frequency range, the R2PI spectra of the ProTrp conformers closely resemble the corresponding spectra of GlyTrp,[31,35] except for a smaller spacing in the ro-vibronic progression of conformer A, so one might expect similar IR spectra and structures as well.

Figure 3 shows the IR−UV hole burning spectra of both conformers of ProTrp in the near and mid-infrared region, with the UV probe laser tuned to 34719 and 34861 cm^{-1} for conformer A and B, respectively. UV frequencies were calibrated against R2PI spectra of aniline and compared to literature values.[48] From earlier measurements of the GlyTrp, TrpGly, and TrpGlyGly systems[30,31] we expect six IR bands with sufficient intensity for detection: three bands between 3200 and 3600 cm^{-1} and another three between 1500 and 1800 cm^{-1}. Namely, they are the O−H stretch vibration of the carboxyl group of the tryptophane residue (OH), the N−H stretch vibration of the indole group (NH_{ind}), the N−H stretch vibration of the peptide bond (NH_{pep}), the C═O stretch vibrations of the carboxyl group (CO(OH)) and peptide bond (CO_{pep}), and the N−H in-plane-bend vibration of the peptide bond (NH_{ipb}). We did not observe the N−H stretch vibration of the pyrrolidine ring, which has a low calculated infrared absorption intensity (see calculations). Table 1 summarizes the observed absorption maxima and tentative assignments.

When looking at the infrared spectra in Figure 3 one first notices that the CO_{pep} band of conformer A seems to be very weak, if visible at all (dashed line). We might assign the reproducible structure around 1648 cm^{-1} to the CO_{pep} band, but the difference between IR−UV and reference signal is quite small and within the noise limits of our measurements. At that wavenumber, we observe strong atmospheric absorptions of the mid-IR beam due to the water bending vibration in air (see experimental section) and the IR pulse energy drops down to ∼50 μJ. The lack of sufficient energy might be the main reason for the weakness of the CO_{pep} band of conformer A. All other bands have frequencies next to or in between water absorptions. Currently we are preparing a purging system to remove the gaseous water from the beam path. However, we cannot rule out intrinsic effects (e.g., a special conformation of the molecule) as a source for the weakness of the band. We tried to normalize the mid-infrared spectra to the IR laser energy in order to compensate in part for water absorptions, but the signal-to-noise ratio around 1648 cm^{-1} is too low to be improved by the normalization.

The spectral assignment, as indicated in Figure 3 and Table 1, is based mainly on the comparison with infrared spectra of GlyTrp and TrpGly.[30,31] Conformer A shows no OH band around 3585 cm^{-1}, indicating that the OH group is bound via a hydrogen bond to the backbone. If the assignment of the CO_{pep} band is correct, this would match to the red shift of the CO_{pep} frequency relative to conformer B, and the OH group is most likely bound to the CO_{pep} group. According to calculations (Table 1 and refs 8 and 31), the absorption of such a hydrogen-bonded OH group is shifted below 3200 cm^{-1}. However, the hydrogen-bonded OH group has never been observed experimentally,[31] probably due to a broadening of the absorption of hydrogen-bonded OH groups.[49] We did not observe any other band between 3200 and 3700 cm^{-1}.

Surprisingly, the NH_{pep} band is red-shifted as well: to near 3300 cm^{-1}. From previous studies[7,31,32,50] one would expect such a large shift only for *strongly* hydrogen-bonded NH groups of

the peptide bond or indole side chain; like in single or multiple (repeated) γ-turns. Since the NH_{ind} band of ProTrp is observed at its *normal*, unbound position (around 3520 cm^{-1}), the band at 3304 cm^{-1} has to be the NH_{pep} band (the intensity of the $NH_{proline}$ band being too weak for observation; see next section). However, ProTrp is too small to have a back-folding backbone and does not permit a $NH_{pep}\cdots X$ hydrogen bond. Therefore, we can rule out hydrogen bond formation to be responsible for the large red shift NH_{pep} band. We did not observe any dimer mass signals, so fragmentation of dimers is an unlikely source for the NH_{pep} band. From that could result the observation of a hydrogen-bonded NH_{pep} band of the dimer on the parent mass channel.

Conformer B resembles the spectrum of a stretched or fully extended backbone. The OH band at 3582 cm^{-1} corresponds to a non-hydrogen-bonded OH group, like in all three conformers of TrpGly and conformer B of GlyTrp. Likewise, the CO_{pep} band at 1692 cm^{-1} shows no significant red-shift, so it is not involved in a hydrogen bond. All other bands (NH_{ind}, CO(OH), and NH_{ipb}) are rather insensitive to changes in the conformational structure and resemble those of previous measurements.[30,31]

4. Calculations

Our theoretical approach is intended to explore the properties of different conformers and the influence of structural changes on the spectral fingerprint. Their structures were chosen by chemical intuition, by a combinatorial approach, and by taking into account the forbidden regions of the Ramachandran plot.[45,51] Such an approach will give us an overview of the types of interactions involved and provides a tool to classify the type of interaction by the vibrational frequencies of the NH_{pep}, CO_{pep} and OH vibrations.

All calculations were performed using the Turbomole program package.[52,53,54] In order to maintain compatibility of the data with our previous calculations on tryptophane containing di- and tripeptides[30,31] we used the b3-lyp_Gaussian functional and the 6-31G(d,p) basis set obtained from ref 55. Benchmark calculations on selected systems showed only marginal differences between the results obtained from either the Turbomole or Gaussian[56] program package, so we can use the same and well investigated scaling factors for the calculated harmonic frequencies of tryptophane containing oligopeptides as in our previous work.[30,31]

A total number of 21 different conformers of ProTrp were calculated at the B3LYP/6-31G(d,p) level of theory. Table 2 summarizes the main structural properties as well as the calculated energies ΔE_0 (including zero-point correction) relative to the most stable conformer (pw01) at that level of theory. Some conformers with different starting geometries collapsed to one of these 21 structures and are not listed in Table 2. φ, ψ, and χ are the usual dihedral angles used to describe the conformational landscape of polypeptides[2,45,51] and are depicted in Figure 1. Since the residues are counted from the nitrogen (NH_2) end, subscripts 1 and 2 refer to the proline (Pro) and tryptophane (Trp) subunits, respectively. α is the dihedral angle of the OH group of the carboxyl group measured relative to the C=O bond. As usual, the peptide bond was kept in trans conformation ($\omega = 180°$) in the starting geometries and did not change much upon geometry optimization. Figure 4 depicts the molecular structures of the 12 most stable conformers of ProTrp.

The conformers are labeled in the one letter code (pw) and consecutively numbered with respect to an ascending DFT energy. Three letters in square brackets are used to indicate the specific conformation. The first letter describes the local conformation of the proline residue (see below). For the local conformation of the tryptophane residue we adopted the nomenclature according to its position in the Ramachandran plot (e.g., γ_L, γ_D, β_L, δ_L, ϵ_L). Finally, the third letter indicates the position of the indole side chain: anti (a, $\chi_{1,2} \sim 180°$), gauche plus (g+, $\sim +60°$), and gauche minus (g−, $\sim -60°$). $\chi_{2,2}$ is almost always $\pm 90°$ in proteins[57] and was kept at $-90°$ in this study.

TABLE 2: Dihedral Angles (in deg) and Relative Energies (in kJ mol^{-1}) of the Calculated Structures [B3LYP/6-31G(d,p)] of ProTrp

conformer	φ_1[a]	ψ_1[a]	φ_2[a]	ψ_2[a]	$\chi_{1,2}$[a]	α[b]	ΔE_0[c]
pw01[$n\gamma_L$g+]	−110.5	−4.3	−72.8	56.0	49.1	−178.1	0.0
pw02[$n\gamma_L$g−]	−113.5	0.1	−73.8	58.4	−54.3	177.7	4.8
pw03[$n\gamma_D$g−]	−137.4	12.1	67.4	−53.4	−57.5	−179.1	13.5
pw04[$n\gamma_L$a]	−113.8	1.2	−75.9	67.4	−154.7	171.5	14.4
pw05[$o\gamma_L$g+]	15.8	152.8	−74.4	57.4	47.7	−178.0	14.7
pw06[$n\beta_L$g+]	−139.3	14.3	−162.6	177.7	60.9	0.8	15.2
pw07[$n\epsilon_L$g+]	−111.0	−2.1	−99.2	179.2	63.7	1.3	17.0
pw08[$n\gamma_D$g+]	−101.2	−10.8	42.4	−28.5	55.0	177.9	17.6
pw09[$n\beta_L$a]	−143.6	19.5	−157.9	143.9	−177.9	−4.2	18.4
pw10[$n\gamma_D$a]	−111.7	−1.2	66.6	−59.7	−169.7	−172.1	20.1
pw11[$o\beta_L$g+]	13.3	159.8	−162.0	175.5	61.8	0.2	20.9
pw12[$o\gamma_L$g−]	8.8	159.0	−75.1	61.3	−51.2	176.8	21.4
pw13[$n\epsilon_L$g−]	−142.7	14.8	−111.5	164.1	−66.1	−0.2	22.6
pw14[$o\beta_L$a]	12.4	158.7	−158.6	148.8	−178.1	−4.6	25.2
pw15[$o\beta_L$g−]	−19.9	156.4	−126.7	165.4	−66.2	−0.6	27.9
pw16[$x\gamma_L$g−]	−143.3	93.9	−74.8	59.3	−51.9	177.1	29.7
pw17[$o\gamma_L$a]	19.4	150.2	−76.9	69.2	−154.6	172.1	31.4
pw18[$x\beta_L$g+]	−43.1	−11.3	−159.4	179.9	60.6	0.9	33.2
pw19[$x\beta_L$a]	−44.8	−7.8	−158.8	149.0	−178.1	−4.5	35.1
pw20[$x\beta_L$g−]	−44.8	−16.7	−120.5	167.1	−67.0	−0.2	39.6
pw21[$n\delta_L$a]	−114.5	11.5	−144.6	37.7	−145.6	174.5	40.0

[a] For the definition of dihedral angles see text and Figure 1. [b] Conformation of the carboxyl group (syn, $\alpha \sim 0°$; anti, $\alpha \sim 180°$). [c] Including zero-point vibrational energy.

In a *real* peptide, where the proline residue is preceded by another amino acid, steric effects limit the values of φ_1 to about -60 to $-75°$.[2,51] Such rigid constraints are not valid for ProTrp, because it has only a small secondary NH group. In addition, an inversion of the proline nitrogen has to be considered as well. Starting from a large set of different φ and ψ values, almost all conformers collapsed into two different local conformations of the proline residue. One has a close $NH_{pep}/N_{proline}$ contact with a H···N distance of ∼2.10−2.20 Å, in which the NH_{pep} group is interacting with the lone pair of the proline nitrogen (e.g., pw01, pw02, pw06, and pw07 in Figure 4). In this set of conformers the proline residue has φ_1 and ψ_1 values of $\sim -120°$ and 0°, respectively. The second major type of conformations is characterized by a $CO_{pep}/NH_{proline}$ interaction (also known as C_5 contact) and an O···H distance of ∼2.15−2.25 Å (e.g., pw05, pw11 and pw12). Here the CO_{pep} and $NH_{proline}$ bonds are nearly collinear ($\varphi_1 \sim 0°$, $\psi_1 \sim -155°$). Because the local conformations of the proline residue obtained from our calculations are different from those found in *real* peptides, we label the conformations according to the type of interaction. That is, conformers with $NH_{pep}/N_{proline}$ and $CO_{pep}/NH_{proline}$ interactions are labeled *n* and *o*, respectively (see Table 2). Those with neither kind of interaction are generally labeled *x*.

According to Table 2, three of the four most stable structures in our calculations differ only in the position of the indole side chain. They are characterized by a strong $OH\cdots OC_{pep}$ hydrogen bond and $NH_{pep}/N_{proline}$ contact. In the most stable structures (pw01 and pw02) the indole ring is underneath the backbone,

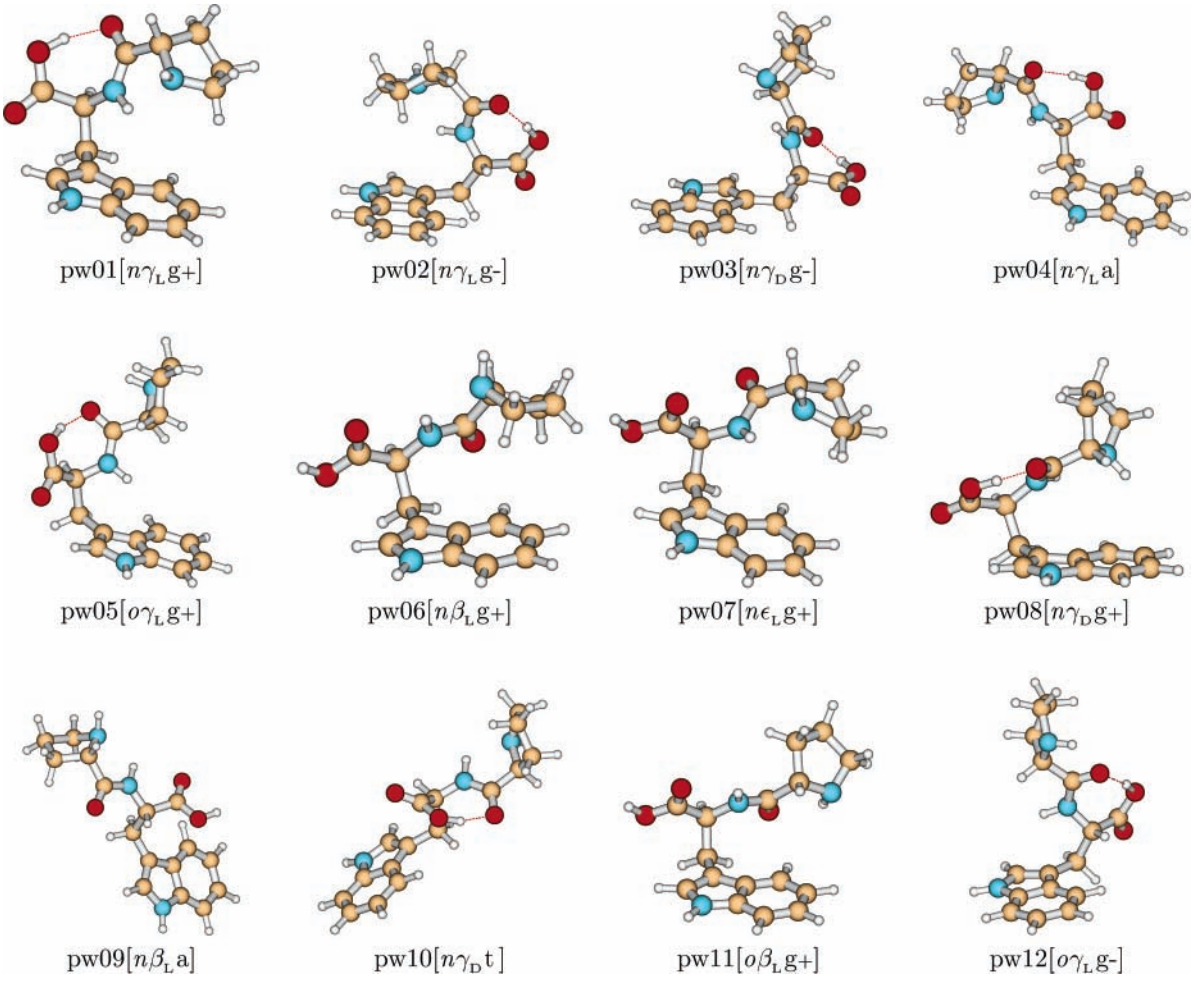

Figure 4. Structures of the 12 most stable conformers [B3LYP/6-31G(d,p)] of ProTrp (see Table 2). At that level of theory, pw01 is the lowest energy conformer and exhibits an OH···OC_{pep} hydrogen bond as well as a $NH_{pep}/N_{proline}$ interaction. Upon explicit inclusion of dispersion interaction [MP2/TZVPP] the energetic order changes and pw02 becomes the most stable conformer (see Figure 5).

while the anti conformation is the least stable (pw04). Analogous results are obtained for other sets of conformers, which also differ only in the position of the indole side chain (e.g., pw05/12/17 and pw11/14/15). Generally g+ conformers are the most stable structures, while anti (a) conformers tend to be the least stable or to have similar energies as g conformers. This implies a significant interaction between indole ring and peptide backbone, although the B3LYP method does not satisfactorily account for dispersion interactions, which are necessary for an adequate description of π interactions (see below).

For otherwise similar conformations, $NH_{pep}/N_{proline}$ interactions are energetically favored over $CO_{pep}/NH_{proline}$ contacts by $\sim$15 kJmol^{-1}. For example, pw01[$n\gamma_L$g+] is more stable than pw05[$o\gamma_L$g+]. Other examples are pw03/pw11 and pw04/pw17. Likewise, $NH_{pep}/N_{proline}$ and $CO_{pep}/NH_{proline}$ interactions are favored over conformations with no such interaction at all (pw18, pw19, pw20). Over all, the proline residue in ProTrp-tends to adopt a local conformation with a $NH_{pep}/N_{proline}$ contact present.

We performed single point calculations and geometry optimizations for the 11 most stable conformers of Table 2 at the RI-MP2/TZVPP level of theory, to get an idea of the importance of dispersion interactions between indole ring and peptide backbone in ProTrp. Figure 5 summarizes the relative energies of the B3LYP/6-31G(d,p) calculations (DFT, left), MP2 single point calculations at the optimized DFT geometries (MP2(SP), middle) and the MP2 geometry optimizations (MP2(Opt), right). For an easier comparison, we arbitrarily chose the energies of the pw04 conformer to be equal in all three types of calculations, because the indole side chain points away from the backbone and dispersion between indole ring and backbone plays a minor role in this conformer.

Figure 5 illustrates perfectly that an explicit inclusion of dispersion at the MP2 level does change the energetic order of the conformers dramatically and that single point calculations at the optimized DFT geometries are not sufficient for an adequate description of the energetic order and relative energies. Now, pw02 is the most stable conformer. The distance between the five-membered pyrrolidine ring and the indole ring decreases by about 1 Å compared to the DFT calculations, while it is increasing by less than 0.1 Å for conformer pw01, which is now the second most stable structure. Both conformers are now much closer in energy and stabilized by dispersion between indole ring and peptide backbone. On the other hand, conformer pw04 is now among the least stable structures, because its geometry (anti conformation of the indole side chain) prohibits such a stabilizing dispersion interaction. In general, the structural changes between DFT and MP2 optimized geometries are rather small, except for a slight contraction of the indole ring/backbone distance in cases where dispersion plays a significant role.

It is interesting to note that conformer pw06, which has no stabilizing OH···OC_{pep} hydrogen bond, but a peptide backbone which is lying on top of the indole ring, is now one of the most stable structures and energetically comparable to pw01 and

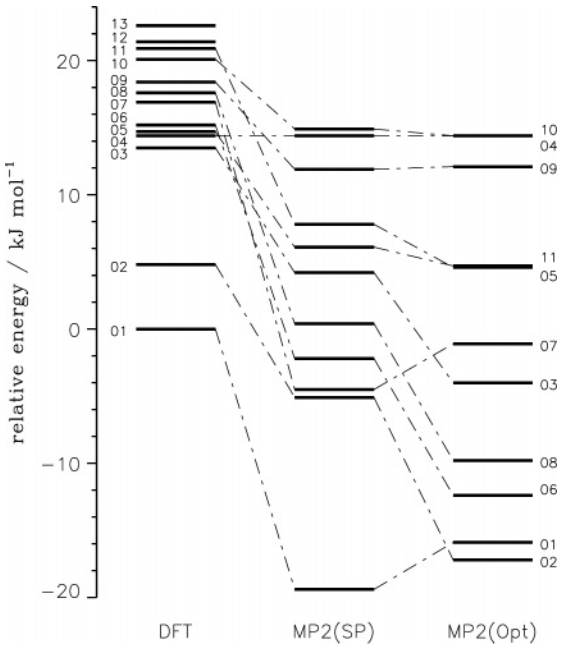

Figure 5. Relative energies of the ProTrp conformers at different levels of theory. The corresponding structures are indicated by their numbers (see Table 2 and Figure 4). DFT: Fully relaxed structures at B3LYP/6-31G(d,p). MP2(SP): Single point calculation at MP2/TZVPP, using the optimized DFT geometries. MP2(Opt): Relative energies of the optimized structures at MP2/TZVPP. (DFT energies include zero-point correction.)

pw02. Although MP2 tends to overestimate dispersion, this indicates the importance of dispersion in calculating energies and structures of different conformers of model peptides.[8] Furthermore, stabilization by dispersion is probably the reason why fully extended (stretched) conformers can be observed in supersonic jets, despite the strong tendency of most model peptides to form hydrogen-bonded γ-turns. This was nicely demonstrated for the H−Trp-Gly−OH system just recently,[8] where only stretched conformers were found experimentally.[30,31]

Table 3 shows the calculated vibrational transition frequencies and infrared intensities of the different ProTrp conformers at the B3LYP/6-31G(d,p) level of theory. Vibrational frequencies are expressed as frequency shifts relative to the pw11 conformer, a stretched conformer with fully extended backbone (ψ_1 and ψ_2 are close to 180°). This way, one can easily identify those vibrations, which are more or less sensitive or insensitive to structural changes. Since conformer pw11 is fully extended, strong hydrogen-bond-like interactions in the different conformers will result in negative values of the frequency shifts (red shift). NH/OH stretch frequencies were scaled by a factor of 0.9546[31] and C═O stretch and N−H in-plane-bend frequencies by 0.964,[30] which are the empirical scaling factors required for the most prominent tryptophane monomer[21] to match the experimental to the calculated indole N−H and carboxylic C═O stretching frequencies.

Table 3 shows that the NH_{ind} and NH_{ipb} vibrations are the least sensitive with regard to structure determination. While NH_{ind} does not shift at all, NH_{ipb} shows larger shifts only for the four least stable conformers. Similarly, the carboxylic C═O stretch vibration is largely insensitive to structural changes, although local β_L conformations of the tryptophane residue mostly result in negative shifts, whereas OH···OC_{pep} hydrogen bonds induce a slight blue shift. However, no strong correlation between conformational structure and vibrational frequency is observable for that band. In contrast, the CO_{pep} vibration exhibits a systematic (and obvious) red-shift of about −40 cm^{-1} upon OH···OC_{pep} hydrogen bond formation, but remains otherwise insensitive. Similarly, the OH stretch vibration is red-shifted by about 400−800 cm^{-1} due to hydrogen bond formation. The previously mentioned CO_{pep}/$NH_{proline}$ interaction has no significant influence on the CO_{pep} vibration.

Among the vibrations listed in Table 3, the NH_{pep} band shows by far the largest effect and is influenced by direct NH···X contacts (e.g., pw06) as well as by indirect interactions via the peptide bond (e.g., pw05), or by both types of interaction (e.g., pw02, pw08). Figure 6 shows the scaled NH_{pep} frequency as a function of the OH stretch frequency. Clearly, four distinct clusters of points can be identified, indicating a systematic correlation between structure and vibrational frequency. The positions of four selected conformers are represented by their numbers. Moving on the abscissa from the right to the left corresponds to the formation of an OH···OC_{pep} hydrogen bond, whereupon the OH frequency shifts to lower wavenumbers. Closer inspection of the calculated structures reveals that the two clusters at the bottom of Figure 6 exhibit exclusively NH_{pep}/$N_{proline}$ interactions, while the top two clusters do not. The four valence dash formulas in Figure 6 depict the basic structural motive of each cluster.

Two major conclusions can be drawn from Figure 6: (1) The NH_{pep} bond is influenced not only by a direct NH_{pep}/$N_{proline}$ interaction, but also indirectly via the peptide bond, when the CO_{pep} group is involved in an OH···OC_{pep} hydrogen bond. Similar effects were observed in previous calculations of conformers of GlyTrp and TrpGly.[31] (2) The frequency shifts of both types of interaction (∼30 and 70 cm^{-1}) are roughly additive. Hence, in the case of ProTrp, the NH_{pep} frequencies could be divided up into four regions, each characterizing a distinct type of interaction with the NH_{pep} bond and peptide group.

There are three points in our present data set that do not fit into the four distinct clusters of points. The first one is conformer pw16, with an OH frequency of about 3260 cm^{-1}. It has an OH···OC_{pep} hydrogen bond, but no NH_{pep}/$N_{proline}$ interaction. The second conformer is pw21, with a NH_{pep} frequency of about 3335 cm^{-1}. This conformer has an OH/π (peptide) and NH_{pep}/$N_{proline}$ interaction, but shows only a small red shift of the OH stretch frequency. However, both conformers still fit into the correlation between NH_{pep} frequency and structure. Finally, pw08 shows the largest red-shift of both the NH_{pep} (3288 cm^{-1}) and OH group (2771 cm^{-1}) and is situated outside the lower left corner of Figure 6. While in all other calculated structures the OH bond is tilted by about 30° against the plane formed by the peptide bond, it is almost coplanar with that plane in pw08 (see Figure 4). The coplanarity provides a better overlap with the lone electron pair on the oxygen atom and leads to a stronger hydrogen bond. However, because of a local γ_D conformation on the tryptophane residue in combination with a g+ conformation of the indole side chain as in pw08, the coplanarity is forced by the repulsion between the indole ring and the CO_{pep} group only. This puts a considerable ring strain on the 7-membered ring formed by the hydrogen bond. Hence, pw08 is energetically less favorable than pw02 or pw01, despite its stronger hydrogen bond (see Figure 5).

The NH stretch vibration of the proline residue might be another sensitive probe of molecular structure. The $NH_{proline}$ frequency shift mainly follows that of the NH_{pep} group, but with opposite sign. Unfortunately, as is evident from Table 3, the infrared intensity is too low to be detected in our experiment.

TABLE 3: Vibrational Frequency Shifts (in cm^{-1}), Relative to Conformer pw11, of the Calculated Structures [B3LYP/6-31G(d,p)] of ProTrp[a]

conformer	NH_{ipb}	CO_{pep}	CO(OH)	$NH_{proline}$	NH_{pep}	NH_{ind}	OH
pw01[$n\gamma_L$g+]	$2_{(351)}$	$-46_{(290)}$	$3_{(296)}$	$93_{(5)}$	$-110_{(147)}$	$-4_{(73)}$	$-523_{(703)}$
pw02[$n\gamma_L$g−]	$2_{(342)}$	$-38_{(279)}$	$15_{(337)}$	$88_{(5)}$	$-107_{(98)}$	$-2_{(68)}$	$-522_{(782)}$
pw03[$n\gamma_D$g−]	$23_{(296)}$	$-38_{(229)}$	$16_{(332)}$	$51_{(6)}$	$-86_{(126)}$	$-1_{(67)}$	$-495_{(694)}$
pw04[$n\gamma_L$a]	$1_{(361)}$	$-37_{(234)}$	$17_{(311)}$	$86_{(4)}$	$-87_{(136)}$	$-1_{(67)}$	$-414_{(642)}$
pw05[$o\gamma_L$g+]	$4_{(342)}$	$-46_{(191)}$	$9_{(289)}$	$18_{(18)}$	$-30_{(165)}$	$-4_{(75)}$	$-425_{(590)}$
pw06[$n\beta_L$g+]	$-10_{(344)}$	$5_{(214)}$	$4_{(194)}$	$39_{(0)}$	$-63_{(94)}$	$0_{(70)}$	$0_{(67)}$
pw07[$n\epsilon_L$g+]	$-8_{(243)}$	$24_{(268)}$	$13_{(204)}$	$92_{(3)}$	$-75_{(97)}$	$-1_{(74)}$	$-3_{(55)}$
pw08[$n\gamma_D$g+]	$42_{(141)}$	$-32_{(280)}$	$-2_{(351)}$	$76_{(10)}$	$-167_{(151)}$	$-2_{(76)}$	$-815_{(1268)}$
pw09[$n\beta_L$a]	$-13_{(405)}$	$11_{(234)}$	$-8_{(174)}$	$37_{(0)}$	$-56_{(99)}$	$0_{(73)}$	$-10_{(46)}$
pw10[$n\gamma_D$a]	$17_{(313)}$	$-37_{(183)}$	$22_{(284)}$	$84_{(3)}$	$-106_{(198)}$	$1_{(72)}$	$-500_{(773)}$
pw11[$o\beta_L$g+]	$0_{(240)}$	$0_{(172)}$	$0_{(196)}$	$0_{(30)}$	$0_{(58)}$	$0_{(71)}$	$0_{(70)}$
pw12[$o\gamma_L$g−]	$-4_{(313)}$	$-38_{(173)}$	$19_{(324)}$	$28_{(21)}$	$-34_{(98)}$	$-2_{(76)}$	$-429_{(681)}$
pw13[$n\epsilon_L$g−]	$-7_{(334)}$	$28_{(201)}$	$7_{(258)}$	$36_{(0)}$	$-48_{(91)}$	$1_{(65)}$	$-4_{(57)}$
pw14[$o\beta_L$a]	$-6_{(289)}$	$6_{(183)}$	$-12_{(196)}$	$5_{(34)}$	$-5_{(53)}$	$-1_{(74)}$	$-8_{(52)}$
pw15[$o\beta_L$g−]	$-2_{(222)}$	$24_{(162)}$	$-5_{(250)}$	$1_{(32)}$	$-10_{(44)}$	$-1_{(70)}$	$-7_{(66)}$
pw16[$x\gamma_L$g−]	$-3_{(348)}$	$-31_{(189)}$	$15_{(346)}$	$35_{(0)}$	$-41_{(113)}$	$-1_{(73)}$	$-502_{(846)}$
pw17[$o\gamma_L$a]	$-3_{(316)}$	$-38_{(146)}$	$20_{(298)}$	$13_{(18)}$	$11_{(33)}$	$-1_{(71)}$	$-324_{(517)}$
pw18[$x\beta_L$g+]	$-16_{(252)}$	$2_{(192)}$	$-6_{(195)}$	$120_{(2)}$	$4_{(46)}$	$-1_{(70)}$	$-1_{(72)}$
pw19[$x\beta_L$a]	$-22_{(287)}$	$6_{(209)}$	$-14_{(188)}$	$121_{(1)}$	$12_{(38)}$	$0_{(75)}$	$-8_{(51)}$
pw20[$x\beta_L$g−]	$-19_{(213)}$	$28_{(186)}$	$-7_{(246)}$	$122_{(4)}$	$3_{(36)}$	$1_{(67)}$	$-5_{(65)}$
pw21[$n\delta_L$a]	$-42_{(375)}$	$30_{(177)}$	$35_{(251)}$	$83_{(4)}$	$-118_{(155)}$	$0_{(65)}$	$-37_{(98)}$

[a] Calculated infrared intensities (km/mol) are given as subscripts in parentheses. NH/OH stretch frequencies were scaled by 0.9546, before calculating the frequency shifts. All other frequencies were scaled by 0.964. Scaled vibrational transition frequencies (in cm^{-1}) for conformer pw11: NH_{ipb}, 1499; CO_{pep}, 1690; CO(OH), 1774; $NH_{proline}$, 3325; NH_{pep}, 3455; NH_{ind}, 3523; OH, 3586.

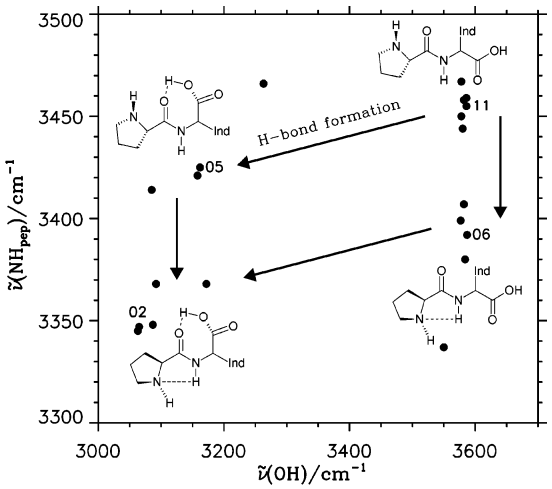

Figure 6. Correlation between NH_{pep} and OH stretch frequencies (scaled) of the different calculated conformers of ProTrp. The pattern is dominated by two types of interactions, namely an OH···OC_{pep} hydrogen bond and a lose $NH_{pep}/N_{proline}$ contact. Four insets in the plot corners indicate the corresponding conformation of the backbone. Numbers indicate the position of four selected conformers in Figure 4. Because of its large OH frequency shift, conformer pw08 is situated at the lower left corner but not visible in the plot.

Also, that very same band is absent in a peptide, where the proline residue is preceded by another amino acid.

5. Discussion

Using the vibrational assignment (Table 1) of the experimental IR/UV spectra in Figure 3, we attempt to characterize the conformational structures of conformers A and B by comparison with the DFT calculations in Table 3. Any possible structure of conformer A has to meet at least two criteria: (1) The OH group must be involved in a hydrogen bond, because we do not observe the free OH band around 3585 cm^{-1}. Since the CO_{pep} bond is the only accessible acceptor site, this implies a red shift of the CO_{pep} band as well, although our interpretation of the weak feature at 1648 cm^{-1} could be challenged. (2) The NH_{pep} band must experience a strong red shift by about 150 cm^{-1} compared to a structure with a fully extended backbone ($\nu(NH_{pep}^{free}) \sim 3450$ cm^{-1} [7,31]), indicating a kind of strong interaction with the NH_{pep} group or peptide bond. Basically, these criteria would put conformer A into the lower left corner in Figure 6.

According to Table 3, of the most stable structures only pw01, pw02, and pw08 fulfill the criteria mentioned above and match the experimental spectra with reasonable accuracy. Figure 3 shows the calculated and scaled stick spectra of pw01, pw02, and pw08 at the DFT level of theory (black) beneath the IR/UV spectrum of conformer A, sorted according to an increasing relative energy at the MP2 level of theory. pw01 and pw02 differ only in the conformation of the indole side chain (g+ vs g−), but are otherwise the same. Consequently, their calculated IR spectra are nearly identical and indistinguishable at the current level of theory and in the spectral region of interest.

However, experimental and calculated NH_{pep} frequencies differ by about 40 cm^{-1}. The experimental NH_{pep} frequency (3304 cm^{-1}) is red-shifted by about 150 cm^{-1} with respect to a free NH_{pep} group. A shift of this size is well-known in structures with single or repeated γ-turns, where the NH_{pep} group itself is the donor in a (strong) hydrogen bond,[32,7] but conformer A does not permit this type of hydrogen bond, due to structural constraints. On the other hand, structure pw08 does account for the strong red-shift of the NH_{pep} band because of its stronger hydrogen bond (Figure 3), but shows a blue shift of the NH_{ipb} absorption to about 1540 cm^{-1}, which we do not observe experimentally. Therefore, it is reasonable to assign conformer A to a structural motif like pw01 or pw02, which are the two most stable conformers in our data set.

On the basis of the DFT calculations, the shift of the NH_{pep} band originates mainly from the combination of an OH···OC_{pep} hydrogen bond and $NH_{pep}/N_{proline}$ contact, where the influence of the latter is the largest; similar to conformer A of the natural dipeptide GlyTrp.[31] It should be noted that this type of interaction is not present in proteins because the secondary nitrogen atom of the proline residue is no longer sp^3 hybridized and the lone electron pair no longer accessible for the neighboring NH_{pep} bond. An additional contribution to the frequency

shift probably stems from a dispersive interaction with the indole ring lying underneath the peptide bond and proline moiety. Such interactions are poorly described at the B3LYP level of theory and might account for the present differences between theory and experiment.

We did calculate harmonic frequencies of the three most stable conformers pw02, pw01, and pw06 at the MP2/TZVPP level of theory, though the calculation is quite expensive. Appropriately scaled stick spectra are also displayed in Figure 3 (red); NH/OH stretch frequencies were scaled by 0.9552 and C═O/NH_{ipb} frequencies by 0.9833 to match the experimental NH_{ind} and CO(OH)frequencies of tryptophane. We observe a blue shift of all frequencies, relative to the corresponding DFT calculations, but not for the NH_{pep} vibrational stretch frequency of pw01 and pw02, which is red-shifted. So the large red shift of the NH_{pep} frequency may be caused in part by dispersion interactions in addition to an OH···OC_{pep} hydrogen bond and $NH_{pep}/N_{proline}$ contact.

Conformer B differs from conformer A in that it has no hydrogen-bonded OH, since we observe the free OH group at 3582 cm^{-1}. Consequently, the CO_{pep} band is not red-shifted and appears at a typical frequency of free CO_{pep} groups around 1690 cm^{-1}.[30] In addition, the NH_{pep} band is red-shifted by about 80 cm^{-1} compared to a structure with an extended backbone. Among the lowest energy structures, only pw06 and pw07 fulfill the above conditions. pw06 fits best to the experimental spectrum of conformer B and is by 24.5 $kJmol^{-1}$ more stable than pw07 at the MP2/TZVPP level of theory (Figure 5). Figure 3 shows the calculated and scaled stick spectra of pw06 and pw07 beneath the IR/UV spectrum of conformer B. Also shown is the calculated stick spectrum of structure pw06 at the MP2 level of theory, which is similar to the DFT result. Hence, we assign conformer B to structure pw06.

Considering the φ, ψ values, both conformers A and B of H−Pro-Trp−OH adopt an α-like local conformation of the proline residue. Mons and co-workers measured the IR/UV spectra of *N*-Acetyl-Phe-Pro−NH_2 and *N*-Acetyl-Pro-Phe−NH_2 and found that the proline residue prefers to adopt a local γ_L conformation in the major conformers.[7,32] The γ_L conformation is stabilized by an NH($i \pm 1$)···CO($i \mp 1$) hydrogen bond, where i is the number of the proline residue. Similar observations were made by Compagnon et al. for Z-Pro−NHMe.[29] This is confirmed by ab initio calculation of isolated YCO−Pro−X model dipeptides (Y = H, Me; X = NH_2, NHMe) in vacuo,[15−17,32] whereas in aqueous solutions α_L and ϵ_L conformations become more stable.[15] The natural dipeptide H−Pro-Trp−OH in our work does not permit the formation of a NH($i \pm 1$)···CO($i \mp 1$) hydrogen bond because of the missing half residue at the proline end, and is therefore unlikely do adopt a local γ_L conformation of the proline residue, but the flexibility of the carboxylic OH group leads to a local γ conformation of the tryptophane residue in conformer A.

These examples demonstrate the high sensitivity of the backbone conformation to the model peptide's structure and to the influence of end groups on the local conformation, whether it is the *normal* end group of a natural peptide or an *artificial* end group in capped peptides. In most cases, γ turns are formed, which directly involve one of the end groups of the model peptide, like the COOH group in natural peptides[31] or the NH_2 or NHMe groups in capped (amidated) peptides.[7,29,32,33] This is not surprising because the hydrogen-bonded structures correspond to the most stable conformers in the gas-phase. In our case, the most stable ProTrp conformer has indeed a local γ-conformation of the tryptophane subunit and the α-conformation of the proline unit is favored due to the stability of the $NH_{pep}/N_{proline}$ contact.

However, the most stable hydrogen bonded conformer is not necessarily the major conformer in supersonic expansions. In some cases (TrpGly, TrpPro, and TrpSer), hydrogen bonded conformers were not observed at all.[30,31,58] As was demonstrated by Valdes et al.[8] and our own work (Figure 5), stretched (fully extended) conformers are stabilized by dispersion interaction between peptide backbone and indole side chain and comparable in energy to the most stable hydrogen-bonded structures. The observation of fully extended conformers in all of our studies of natural peptides[30,31,58] supports this conclusion (e.g., conformer B and structure pw06 in this work). This and the apparent sensitivity of the local conformation to the type of end groups of the model peptide might stimulate further theoretical work on these kind of systems. With the number of experimentally investigated systems rapidly increasing, they provide us both with the necessary data to improve theory and a good reason to study many different small model systems in order to predict the behavior of larger biological systems.

The question remains why, in some cases, we do not observe the hydrogen bonded (stabilized) conformer (e.g., TrpGly). And why we do not observe both of the two most stable conformers of ProTrp, namely pw01 and pw02, which differ only by 1.3 $kJmol^{-1}$ in energy. UV/UV double resonance spectra revealed only two conformers in supersonic expansions ProTrp.[35] Since the structures are very similar, we would expect both conformers to absorb in the same spectral region, but we cannot rule out different lifetimes in the electronically excited-state or unfavorable Franck−Condon factors as a cause for not observing one of the conformers by REMPI spectroscopy. Also, supersonic expansions combined with laser desorption sources start from a hot nonequilibrium condition and conformational relaxation is hindered by the rapid cooling and limited number of collisions in the expansion. So it is not uncommon to observe other conformers than the global equilibrium structures in these types of experiments.

It is interesting to note that, although proline exists in γ formation,[51,59] the vast majority of proline residues in proteins belong to the α and polyproline II (ϵ_L) regions of the Ramachandran plot.[2,51,60] Furthermore, γ-turns seem to be rare compared to β-turns, because of the rather strained geometry of the former.[1,51] So far, we are only starting to understand more common types of turns[7,13,14] as well as β-sheets[38−43] and helices.[12,28,34] In the future, we might have to consider ways to influence the abundance of specific structural motifs in our measurements, in order to study and understand a larger variety of motifs in the gas-phase.[61−63]

6. Summary

On the basis of our DFT calculations, we tentatively assign conformers A and B of ProTrp to structures pw01/pw02 and pw06, respectively (Figure 4). They only differ in the formation of an OH···OC_{pep} hydrogen bond in conformer A, but adopt the same local conformation of the proline residue and orientation of the indole side chain relative to the backbone. Both structures have a favorable $NH_{pep}/N_{proline}$ interaction, causing a red shift of the NH_{pep} band, which is enhanced by the OH···OC_{pep} hydrogen bond in conformer A. Furthermore, dispersive interactions play a major role in the relative stability of the different conformers as well as the NH_{pep} frequency in cases where the NH_{pep} bond interacts with the indole side chain. Single point MP2 calculations at the optimized DFT structures are not sufficient to describe the energetic order in these systems.

Finally, the local conformations of the peptide residues depend strongly on the specific type of model system and its end groups.

Acknowledgment. We thank M. Gerhards and M. Schmitt for fruitful discussions. This work has been supported by the Deutsche Forschungsgemeinschaft (Kl 531/26).

References and Notes

(1) Richardson, J. *Adv. Protein Chem.* **1981**, *34*, 167−339.
(2) Creighton, T. E. *Proteins: structures and molecular properties*, 2nd ed.; W. H. Freeman and Company: San Francisco, CA, 1993.
(3) Simons, J. P. *C. R. Chim.* **2003**, *6*, 17−31.
(4) Robertson, E.; Simons, J. *Phys. Chem. Chem. Phys.* **2001**, *3*, 1−18.
(5) Zwier, T. *J. Phys. Chem. A* **2001**, *105*, 8827−8839.
(6) Weinkauf, R.; Schermann, J.-P.; de Vries, M.; Kleinermanns, K. *Eur. Phys. J. D* **2002**, *20*, 309−316.
(7) Chin, W.; Piuzzi, F.; Dimicoli, I.; Mons, M. *Phys. Chem. Chem. Phys.* **2006**, *8*, 1033−1048.
(8) Valdés, H.; Řeha, D.; Hobza, P. *J. Phys. Chem. B* **2006**, *110*, 6385−6396.
(9) Řeha, D.; Valdés, H.; Vondrášek, J.; Hobza, P.; Abu-Riziq, A.; Crews, B. and de Vries, M. *Chem.—Eur. J.* **2005**, *11*, 6803−6817.
(10) Abo-Riziq, A.; Bushnell, J.; Crews, B.; Callahan, M.; Grace, L. and de Vries, M. *Int. J. Quantum Chem.* **2005**, *105*, 437−445.
(11) Jalkanen, K.; Elstner, M.; Suhai, S. *J. Mol. Struct.* (THEOCHEM), **2004**, *675*, 61−77.
(12) Perczel, A.; Jákli, I.; Csizmadia, I. *Chem.—Eur. J.* **2003**, *9*, 5332−5342.
(13) Perczel, A.; Jákli, I.; McAllister, M.; Csizmadia, I. *Chem.—Eur. J.* **2003**, *9*, 2551−2566.
(14) Möhle, K.; Hofmann, H.-J. *J. Mol. Model.* **1998**, *4*, 53−60.
(15) Benzi, C.; Improta, R.; Scalmani, G.; Barone, V. *J. Comput. Chem.* **2002**, *23*, 341−350.
(16) Baldoni, H.; Rodriguez, A.; Zamora, M.; Zamarbide, G.; Enriz, R.; Farkas, O.; Csàszàr, P.; Torday, L.; Sosa, C.; Jàkli, I.; Perzel, A.; Papp, J.; Hollosi, M.; Csizmadia, I. *J. Mol. Struct.* (THEOCHEM), **1999**, *465*, 79−91.
(17) Sahai, M.; Kehoe, T.; Koo, J.; Setiadi, D.; Chass, G.; Viskolcz, B.; Penke, B.; Pai, E.; Csizmadia, I. *J. Phys. Chem. A* **2005**, *109*, 2660−2679.
(18) Rizzo, T. R.; Park, Y. D.; Peteanu, L. A.; Levy, D. H. *J. Chem. Phys.* **1986**, *84*, 2534−2541.
(19) Cable, J.; Tubergen, M.; Levy, D. *J. Am. Chem. Soc.* **1987**, *109*, 6198−6199.
(20) Cable, J.; Tubergen, M.; Levy, D. *J. Am. Chem. Soc.* **1989**, *111*, 9032−9039.
(21) Snoek, L. C.; Kroemer, R. T.; Hockridge, M. R.; Simons, J. P. *Phys. Chem. Chem. Phys.* **2001**, *3*, 1819−1826.
(22) Snoek, L. C.; Kroemer, R. T.; Simons, J. P. *Phys. Chem. Chem. Phys.* **2002**, *4*, 2130−2139.
(23) Snoek, L. C.; Robertson, E. G.; Kroemer, R. T.; Simons, J. P. *Chem. Phys. Lett.* **2000**, *321*, 49−56.
(24) Lee, Y.; Jung, J.; Kim, B.; Butz, P.; Snoek, L.; Kroemer, R.; Simons, J. *J. Phys. Chem. A* **2004**, *108*, 69−73.
(25) Dian, B. C.; Longarte, A.; Mercier, S.; Evans, D. A.; Wales, D. J.; Zwier, T. S. *J. Chem. Phys.* **2002**, *117*, 10688−10702.
(26) Bakker, J.; Mac Aleese, L.; Meijer, G.; Von Helden, G. *Phys. Rev. Lett.* **2003**, *91*, 203003/1−203003/4.
(27) Çarçabal, P.; Kroemer, R.; Snoek, L.; Simons, J.; Bakker, J.; Compagnon, I.;. Meijer, G.; Von Helden, G. *Phys. Chem. Chem. Phys.* **2004**, *6*, 4546−4552.
(28) Abo-Riziq, A.; Crews, B.; Callahan, M.; Grace, L.; de Vries, M. *Angew. Chem., Int. Ed. Engl.* **2006**, *45*, 5166−5169.
(29) Compagnon, I.; Oomens, J.; Bakker, J.; Meijer, G.; Von Helden, G. *Phys. Chem. Chem. Phys.* **2005**, *7*, 13−15.
(30) Bakker, J. M.; Plützer, C.; Hünig, I.; Häber, T.; Compagnon, I.; von Helden, G.; Meijer, G.; Kleinermanns, K. *Chem. Phys. Chem.* **2005**, *6*, 120−128.
(31) Hünig, I.; Kleinermanns, K. *Phys. Chem. Chem. Phys.* **2004**, *6*, 2650−2658.
(32) Chin, W.; Mons, M.; Dognon, J.-P.; Piuzzi, F.; Tardivel, B.; Dimicoli, I. *Phys. Chem. Chem. Phys.* **2004**, *6*, 2700−2709.
(33) Chin, W.; Piuzzi, F.; Dognon, J.-P.; Dimicoli, I.; Mons, M. *J. Chem. Phys.* **2005**, *123*, 1−11.
(34) Chin, W.; Piuzzi, F.; Dognon, J.-P.; Dimicoli, I.; Tardivel, B.; Mons, M. *J. Am. Chem. Soc.* **2005**, *127*, 11900−11901.
(35) Hünig, I.; Seefeld, K. A.; Kleinermanns, K. *Chem. Phys. Lett.* **2003**, *369*, 173−179.
(36) Cohen, K.; Brauer, B.; Nir, E.; Grace, L.; De Vries, M. *J. Phys. Chem. A* **2000**, *104*, 6351−6355.
(37) Fricke, H.; Gerlach, A.; Unterberg, C.; Rzepecki, P.; Schrader, T.; Gerhards, M. *Phys. Chem. Chem. Phys.* **2004**, *6*, 4636−4641.
(38) Gerhards, M.; Unterberg, C. *Phys. Chem. Chem. Phys.* **2002**, *4*, 1760−1765.
(39) Unterberg, C.; Gerlach, A.; Schrader, T.; Gerhards, M. *J. Chem. Phys.* **2003**, *118*, 8296−8300.
(40) Unterberg, C.; Gerlach, A.; Schrader, T.; Gerhards, M. *Eur. Phys. J. D* **2002**, *20*, 543−550.
(41) Gerhards, M.; Unterberg, C.; Gerlach, A. *Phys. Chem. Chem. Phys.* **2002**, *4*, 5563−5565.
(42) Gerhards, M.; Unterberg, C.; Gerlach, A.; Jansen, A. *Phys. Chem. Chem. Phys.* **2004**, *6*, 2682−2690.
(43) Fricke, H.; Gerlach, A.; Gerhards, M. *Phys. Chem. Chem. Phys.* **2006**, *8*, 1660−1662.
(44) Balbach, J.; Schmid, F. X. Proline isomerization and its catalysis in protein folding. In *Mechanisms of Protein Folding*, 2nd ed.; Pain, R. H., Ed.; Oxford University Press: Oxford, U.K., 2000.
(45) Edsall, J. T.; Flory, P. J.; Kendrew, J. C.; Liquori, A.; Némethy, G.; Ramachandran, G.; Scheraga, H. *J. Biol. Chem.* **1966**, *241*, 1004−1008.
(46) Janzen, C.; Spangenberg, D.; Roth, W.; Kleinermanns, K. *J. Chem. Phys.* **1999**, *110*, 9898−9907.
(47) Gerhards, M. *Opt. Commun.* **2004**, *241*, 493−497.
(48) Mikami, N.; Hiraya, A.; Fujiwara, I.; Ito, M. *Chem. Phys. Lett.* **1980**, *74*, 531−535.
(49) Imhof, P.; Roth, W.; Janzen, C.; Spangenberg, D.; Kleinermanns, K. *Chem. Phys.* **1999**, *242*, 153−159.
(50) Gerlach, A.; Unterberg, C.; Fricke, H.; Gerhards, M. *Mol. Phys.* **2005**, *103*, 1521−1529.
(51) Lovell, S.; Davis, I.; Arendall, W., III; De Bakker, P.; Word, J.; Prisant, M.; Richardson, J.; Richardson, D. *Proteins: Struct., Function, Genetics* **2003**, *50*, 437−450.
(52) Treutler, O.; Ahlrichs, R. *J. Chem. Phys.* **1995**, *102*, 346−354.
(53) Deglmann, P.; Furche, F.; Ahlrichs, R. *Chem. Phys. Lett.* **2002**, *362*, 511−518.
(54) Deglmann, P.; Furche, F. *J. Chem. Phys.* **2002**, *117*, 9535−9538.
(55) http://www.emsl.pnl.gov/forms/basisform.html.
(56) Frisch, M. J.; et al. Gaussian 98, Revision A.9, Gaussian, Inc.: Pittsburgh PA, 1998.
(57) Lovell, S.; Word, J.; Richardson, J.; Richardson, D. *Proteins: Struct., Function Genetics* **2000**, *40*, 389−408.
(58) Seefeld, K.; Häber, T.; Kleinermanns, K. IR/UV spectra of TrpPro and TrpSer, manuscript in preparation, 2006.
(59) Guruprasad, K.; Prasad, M.; Kumar, G. *J. Peptide Res.* **2000**, *56*, 250−263.
(60) Guruprasad, K.; Pavan, M.; Rajkumar, S.; Swaminathan, S. *Curr. Sci.* **2000**, *79*, 992−994.
(61) Clarkson, J.; Baquero, E.; Shubert, V.; Myshakin, E.; Jordan, K.; Zwier, T. *Science* **2005**, *307*, 1443−1446.
(62) Clarkson, J.; Dian, B.; Moriggi, L.; Defusco, A.; McCarthy, V.; Jordan, K.; Zwier, T. *J. Chem. Phys.* **2005**, *122*, 1−15.
(63) Zwier, T. *J. Phys. Chem. A* **2006**, *110*, 4133−4150.